Journal of Magnetic Resonance **148,** 267–276 (2001)
doi:10.1006/jmre.2000.2244, available online at http://www.idealibrary.com on IDEAL®

NMR Paramagnetic Relaxation Enhancement: Test of the Controlling Influence of ZFS Rhombicity for $S = 1$

J. C. Miller, L. L. Lohr, and R. R. Sharp[1]

Department of Chemistry, University of Michigan, Ann Arbor, Michigan 48109

Received March 29, 2000; revised October 30, 2000

Prior theoretical work has predicted that the NMR paramagnetic relaxation enhancement (NMR-PRE) produced by electron spin $S = 1$ ions is highly sensitive to orthorhombic terms in the static zero field splitting (zfs) tensor. Zfs orthorhombicity (which implies chemical inequivalence of the three principal directions of the zfs-principal axis system and is described by the zfs E-parameter) is predicted to suppress the NMR-PRE profoundly relative to the reference cylindrical zfs-limit situation. This expectation was tested experimentally by a comparison of the zfs-limit NMR-PRE produced by $[Ni(II)(en)_3]^{2+}$ (en = ethylenediamine), a trigonal complex which lacks zfs-rhombicity, with the zfs-limit NMR-PRE produced by two orthorhombic complexes, $[Ni(II)(en)_2(H_2O)_2]^{2+}$ and $[Ni(II)(en)(H_2O)_4]^{2+}$. As predicted, the zfs-limit NMR-PRE produced by the orthorhombic complexes in the proton resonance of a dioxane probe species in the solvent was strongly suppressed (by factors of approximately 5 and 7, respectively) relative to the comparable measurement on the trigonal complex. The suppression of the NMR-PRE due to the orthorhombic zfs terms is counteracted by an applied Zeeman field, leading to a predicted rise in the NMR-PRE with increasing Zeeman field strength; this rise occurs when the Zeeman energy is comparable to the orthorhombic zfs splitting, $2E$. This second prediction of theory was likewise confirmed: the expected rhombicity-induced magnetic field dependence in the NMR-PRE was observed for the orthorhombic complexes but not for the trigonal complex. © 2001 Academic Press

Key Words: **paramagnetic NMR; relaxation; zfs; zero field splitting; rhombicity.**

INTRODUCTION

NMR relaxation rates in solution phase are often enhanced profoundly by the presence of dissolved paramagnetic solutes. This phenomenon, called NMR paramagnetic relaxation enhancement or NMR-PRE, has been used widely as a spectroscopic probe of quite diverse chemical and physical phenomena involving molecular structure, solution dynamics, magnetic properties, and the kinetics of ligand exchange reactions. The NMR-PRE produced by electron spin-1/2 species is well understood theoretically and is described by the widely used theory of Solomon, Bloembergen and Morgan (*1–3*) (SBM theory). The NMR-PRE produced by metal ions with electron spin $S \geq 1$ is much more complex due to the influence of competing Zeeman and zero field splitting (zfs) interactions in the electron spin Hamiltonian. The zfs interaction arises from an interplay of electron spin and orbital angular momenta mediated by spin–orbit coupling. The zfs contribution to the energy, which is usually calculated by second-order perturbation theory, is (very roughly) of comparable magnitude to the electronic Zeeman interaction at the typical laboratory magnetic field strengths of NMR spectroscopy. By varying the Zeeman field strength, it is often possible to conduct NMR relaxation experiments over a range of field strengths corresponding, at the low end, to the zfs-limit, where the zfs Hamiltonian is much larger than the Zeeman Hamiltonian ($H_{zfs} \gg H_{Zeem}$), up to, at the high end, the Zeeman-limit, where $H_{Zeem} \gg H_{zfs}$. The data in such experiments is usually presented as a magnetic field dispersion profile (fdp) of the NMR-PRE.

Ongoing theoretical work in this (*4–13*) and other (*14–23*) laboratories is directed toward understanding the influence of the zfs interaction on the NMR-PRE produced by $S \geq 1$ transition metal complexes. Our recent experimental research (*10, 12, 13, 24, 25*) has been directed at testing experimentally the central predictions of theory. This article reports the results of one such test: namely, that for $S = 1$ it is the zfs rhombicity (described by the ESR E parameter), rather than the larger cylindrical zfs term (the D parameter), that exerts a controlling influence on the magnitude and magnetic field dependence of the zfs-limit NMR-PRE (*8, 9, 10, 26*). (Zfs orthorhombicity is present when the principal values of the zfs tensor all differ, which occurs when the principal directions, $\hat{x}$, $\hat{y}$, $\hat{z}$, are chemically inequivalent; in the cylindrical zfs case, $\hat{x} = \hat{y} \neq \hat{z}$.) Theory predicts that the orthorhombic zfs components strongly suppress the NMR-PRE in the vicinity of the zfs-limit, relative to the reference situation where the orthorhombic zfs components are zero. The reported experiments involve a comparison of the NMR-PRE produced by three $S = 1$ Ni(II) complexes, in one of which, $[Ni(en)_3]^{2+}$, the Ni(II) ion lies on a threefold symmetry axis (*27*) and orthorhombic zfs tensor components are absent (Fig. 1); in the other two, [*trans*-$Ni(II)(en)_2(H_2O)_2]^{2+}$ and $[Ni(II)(en)(H_2O)_4]^{2+}$, zfs orthorhombicity is present.

The physical basis of the effect of zfs-rhombicity on the

[1] To whom correspondence should be addressed. Fax: (734)-973-4865. E-mail: rrsharp@umich.edu.

1090-7807/01 $35.00

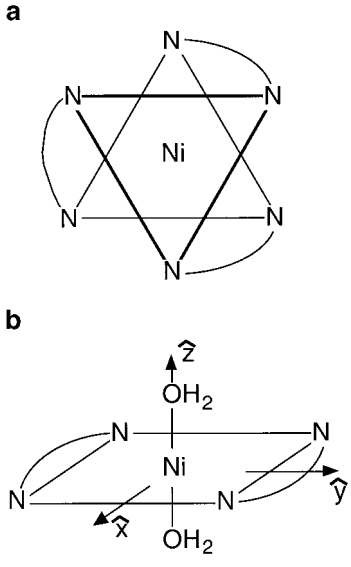

FIG. 1. Schematic models of (a) $[Ni(II)(en)_3]^{2+}$ and (b) $[Ni(II)(en)_2(H_2O)_2]^{2+}$ indicating symmetry of the coordination sphere.

NMR-PRE can be described as follows. Paramagnetic relaxation enhancement depends fundamentally on the electron spin dynamics, both on the coherent spin precessional or oscillational motions and on the electron spin relaxation time, which determine the efficiency of energy transfer between the electron (S) and nuclear (I) spin systems. The coherent spin motions are determined by the spin level structure. For an $S = 1$ spin system of high-spin (Ni(II)), zfs rhombicity splits the $|\pm 1\rangle$ non-Kramers doublet, in consequence inducing oscillation in the time correlation function, $G_z(t) = \langle S_z(0)S_z(t)\rangle$ at a frequency equivalent to the doublet splitting. The rhombicity-induced oscillation in $G_z(t)$ inhibits energy transfer between the electron and nuclear spin systems and is very sensitively reflected in the NMR-PRE, which is profoundly depressed in the vicinity of the zfs-limit. The depression is relieved by an applied Zeeman field when the magnitude of the Zeeman energy is greater than the zfs-limit doublet splitting. Complexes with spin $S = 1$ that possess orthorhombic or cylindrical zfs tensors are thus expected to exhibit very different behavior; the NMR-PRE of orthorhombic complexes is subject to profound rhombicity-induced depression in the low-field limit, rising several-fold with increasing Zeeman field strength when the Zeeman energy exceeds the zfs-limit doublet splitting. These phenomena, which are described in greater detail below, are absent for a cylindrical zfs tensor in which case the $|\pm 1\rangle$ levels are degenerate.

The predicted rise in the T_1 field dispersion profile for orthorhombic Ni(II) complexes has been observed in prior studies (*10, 12, 13, 15, 28, 29*) and constitutes the main characteristic dispersive feature of these profiles. However, parallel studies have not been reported for complexes possessing a cylindrical zfs tensor, where this kind of feature in the fdp is expected to be absent. The results of such a study are reported here.

Experimental Design

The complexes $[Ni(II)(en)_n(H_2O)_{6-2n}]^{2+}$ ($n = 0, 1, 2, 3$; en = ethylenediamine) form a stepwise series, for which formation constants have been measured in aqueous and in mixed water/dioxane solutions (*30*). Two kinds of NMR experiment are reported. In the first, a solution of Ni(II) dissolved in a mixed dioxane/^2H_2O solvent (6 mol% dioxane) was titrated with the bidentate ligand ethylenediamine, and the proton relaxation rate R_1 of the dioxane probe species was measured as a function of the (en)/Ni(II) mole ratio. UV-VIS spectra were recorded in a parallel titration experiment, which showed that dioxane does not enter the Ni(II) coordination sphere, so that the measured R_{1p} (which is the measured T_1 relaxation rate after correction for the diamagnetic background) results solely from an *inter*molecular dipole–dipole relaxation mechanism. The titration experiment was conducted at a Zeeman field strength (0.25 T) which corresponds approximately to the zfs-limit. Using the known stepwise formation constants to calculate concentrations of the four Ni(II)-containing species, zfs-limit NMR relaxivities, $[R_{1p}^{(n)}]_0$, were determined for each complex in the series. The theoretical prediction that $[R_{1p}^{(n)}]_0$ for the orthorhombic (*mono-* and *bis-*(en)) complexes should be several-fold smaller than for the cylindrical (*tris-*(en)) complex was tested and confirmed.

R_{1p} magnetic field dispersion profiles (fdps) of the dioxane probe resonance were then measured for the *bis-* ($n = 2$) and *tris-* ($n = 3$) complexes in the same solvent system. The fdp of the *bis*–(en) complex, which possesses an orthorhombic zfs tensor, is expected theoretically to exhibit a dispersive feature in which R_{1p} rises profoundly (several-fold) with increasing Zeeman field strength in the regime of field strengths where the Zeeman energy is comparable to the orthorhombic zfs splitting of the $m_S = \pm 1$ non-Kramers doublet. The physical origin of this phenomenon is described in greater detail in Discussion. The fdp of the *tris*–(en) complex, which contains no orthorhombic zfs component, is expected not to exhibit this phenomenon.

THEORY

Closed-form expressions have been derived (*5, 10*) for the NMR-PRE in the slow-reorientation situation for both the *intra-* and *inter*molecular relaxation rates in the zfs-limit ($H_{zfs} \gg H_{Zeem}$) and in the intermediate regime ($H_{Zeem} \approx H_{zfs}$). These slow-reorientation expressions are physically appropriate when Brownian reorientation is slow on the time scale of electron spin relaxation ($\tau_R^{(2)} \gg \tau_S$, where $\tau_R^{(2)}$ is the reorientational correlation time for a rank-2 molecule-fixed tensor). For the Ni(II) complexes studied here, τ_S is about threefold shorter than $\tau_R^{(2)}$, but a significant reorientational contribution is still

present, primarily in $\tau_{S,r}$ (see below). The effects of Brownian reorientation can be described using spin dynamics (SD) simulation techniques, which were used in the data analysis.

Spin-Dynamics Simulation Methods

To calculate the NMR-PRE in the intermediate regime where the zfs and Zeeman energies are of arbitrary magnitude and where the paramagnetic solute undergoes rapid Brownian reorientation, SD simulation methods were used as described in Ref. (*25*). The algorithms are implemented in the computer program RotJmpDyn.f, which is a refined and extended version of the program described in Ref. (*11*). SD simulations of the NMR-PRE are analogous in spirit to molecular dynamics (MD) simulations, except that the matrix elements of the electron spin operators are propagated in the time domain using the QM equation of the spin motion rather than, as in MD, propagating molecular coordinates in the time domain using the Newtonian equations of motion. In this way, the fundamental quantities of spin relaxation theory, which are the time correlation functions (TCFs) of the spin operators, $G_r(t) = \overline{\langle S_r(0) \cdot S_r(t)\rangle}$, ($r = 0$, ± 1 or $\hat{x}$, $\hat{y}$, $\hat{z}$), are calculated across a trajectory of finite time steps. The closed-form expression of Torrey (*31*) and Abragam (*32*) was used to describe the translational TCF. SD simulations of the *inter*molecular R_{1p} require a "distance of closest approach" parameter, d_c, which was determined using molecular dynamics simulations procedures implemented in the commercial software package Cerius2 (Biosym/MSD, Inc.).

Electron Spin Relaxation

The electron spin relaxation time was taken as a sum of contributions arising from collisional (*3, 20, 23, 33*) and reorientational (*34*) modulation of the zfs tensor,

$$\tau_S^{-1} = \tau_{S,c}^{-1} + \tau_{S,R}^{-1}. \qquad [1]$$

The effects of $\tau_{S,R}$ are computed directly within the SD algorithms, which compute the motion of the electron spin in the presence of a randomly reorienting spin Hamiltonian. Thus no independent parametrization of this quantity (beyond the static zfs parameters, D and E, and the reorientational correlation time $\tau_R^{(2)}$) is required.

The collisional mechanism ($\tau_{S,c}$) describes electron spin relaxation arising from stochastic modulation of the zfs tensor due to Brownian collisions between free solvent molecules and the metal coordination sphere. This mechanism is described by the Bloembergen and Morgan (B–M) theory (*3*). Taking Δ_t^2 as the trace of the collisionally modulated part of the mean-squared zfs tensor and τ_v as the correlation time for collisional zfs fluctuations, B–M theory gives

$$\tau_{S,c}^{-1} = (\Delta_t^2 \tau_v/5)[1/(1 + \omega_S^2\tau_v^2) + 4/(1 + 4\omega_S^2\tau_v^2)]. \qquad [2]$$

Equation [2] assumes a Zeeman-limit Hamiltonian and $S = 1$. Outside the Zeeman-limit, a realistic description of the magnetic field dependence of $\tau_{S,c}$ requires theory which incorporates the effects of the static zfs interaction in the electron spin Hamiltonian. We have recently developed theory (to be published) which does this in the slow-reorientation situation, $\tau_v \ll \tau_R^{(2)}$, for Zeeman and static zfs interactions of arbitrary magnitude. This theory, which is outlined in the Appendix, is incorporated in the computer program RotJmpDyn.f and was used in the analyses of fdp data that are described below. Bertini *et al.* (*23*) have described a density matrix (DM) calculation of $\tau_{S,c}$, using an approach which, like ours, assumes slow reorientation and is capable of handling regimes where Zeeman and zfs interactions are of arbitrary magnitude. However, the two formulations differ in the basic description of the experiment in that ours involves a calculation of the decay of the time correlation functions, $G_r(t) = \overline{\langle S_r(t) \cdot S_r(0)\rangle}$, ($r = x, y, z$), of the electron spin components in a thermal equilibrium ensemble, while their method calculates the decay of the density matrix. We prefer the former approach, which leads to somewhat different results from DMT, since during NMR relaxation experiments, the electron spin density matrix remains at thermal equilibrium and is not time-dependent. It is the motion of the time correlation functions, $G_r(t)$, rather than that of the density matrix, which appears in NMR relaxation theory. In a strict sense (at least) DMT does not provide a physically appropriate description of the NMR-PRE experiment. SD simulations of $\tau_{S,c}^{-1}$ and $\tau_{S,R}^{-1}$ require specification of the static (B_0, D, E) and dynamic (Δ_T^2, τ_v) electron spin Hamiltonians.

RESULTS

The complexes $[Ni(II)(en)_n(H_2O)_{6-2n}]^{2+}$ ($n = 0, 1, 2, 3$) form a stepwise series. Initial experiments were conducted to determine the molar relaxivity of each complex of the series at a magnetic field strength which corresponds to the vicinity of the zfs-limit. Magnetic field dispersion profile measurements described below demonstrated that a Zeeman field strength of $B_0 = 0.25$ T (10.6-MHz proton frequency) is suitable for this purpose. Theory predicts that the zfs-limit molar relaxivity of the *mono*– and *bis*–en complexes, for which the zfs tensor is orthorhombic, should be much smaller (several-fold) than the zfs-limit relaxivity of the *tris*–en complex, where the coordination sphere is uniaxial. The titration experiments tested this prediction.

The NMR-PRE titration was conducted using the dioxane proton resonance of solutions prepared with a mixed dioxane–^2H_2O (25:75 v/v) solvent. Dioxane is a very weakly coordinating solvent, and in mixed dioxane/water medium we expect that dioxane will not enter the Ni(II) coordination sphere. This point was tested by comparing the UV-VIS spectra of Ni^{2+} in aqueous solution and in the mixed dioxane/water solvent. The spectra were essentially identical, with the three principal

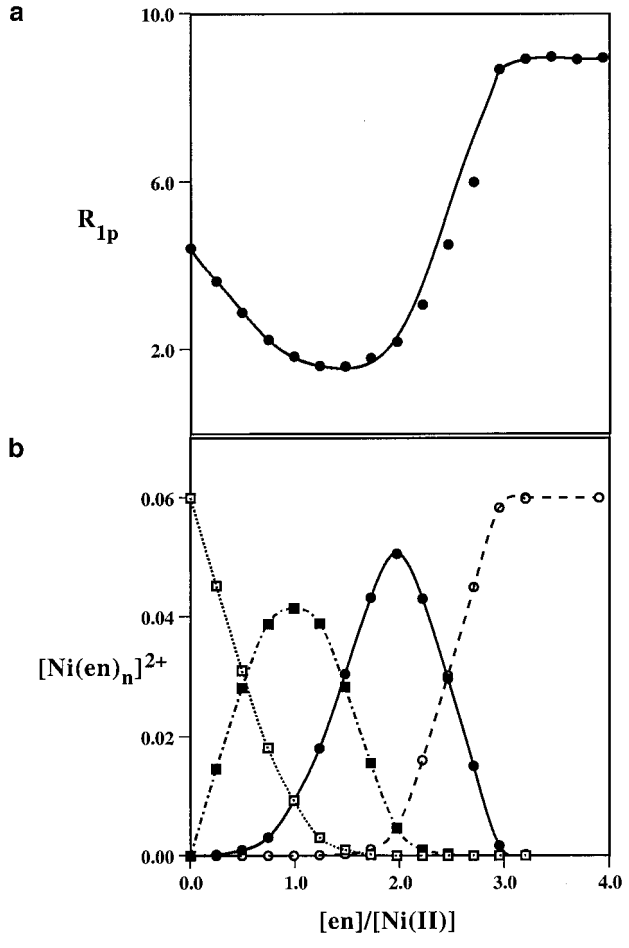

FIG. 2. (a) Results of the R_{1p} titration experiment. R_{1p} (s^{-1}) is the NMR T_1 relaxation rate, corrected for diamagnetic background, of dioxane protons in solutions containing 60 mM $Ni(II)Cl_2$ dissolved in a mixed ^2H_2O/dioxane solvent (75/25 v/v) to which ethylenediamine (en) was added at the indicated stoichiometry (20.0 ± 0.2°C, 10.6 MHz). Solid curve is calculated using the molar relaxivities in Table 1 and the concentrations shown in (b). (b) Concentrations, normalized to 60 mM total Ni(II), of $[Ni(II)(en)_n(H_2O)_{6-2n}]^{2+}$ as a function of the –/[Ni(II)] stoichiometry for $n = 0$ (open squares), 1 (filled squares), 2 (filled circles), and 3 (open circles)). Plotted concentrations were calculated from literature values of the stability constants (see text).

bands unshifted ($\Delta\lambda_{max} < 1$ nm) and with extinction coefficients which differ by <3%. Thus the dioxane proton R_{1p} provides a probe of the *inter*molecular NMR-PRE with little if any *intra*molecular contribution.

The titration was conducted as described above by adding 25-μL aliquots of a stock solution of 15 mM ethylenediamine to a 500-μL NMR sample containing 60 mM $Ni(II)Cl_2$. The dioxane proton R_{1p} was measured after each addition, with results that are shown in Fig. 2a. The results of a parallel UV-VIS titration experiment are shown in Fig. 3a. Shown in Fig. 2b are concentrations of Ni(II) and the three Ni(II)–$(en)_n$ complexes, normalized to 60 mM total Ni(II). These concentrations were calculated by averaging the literature values of the stepwise formation constants measured in aqueous solution and in 12 mol% water/dioxane (*30*). The stepwise formation constants are (with the aqueous number first and the mixed solvent in parentheses): $\log K_1 = 7.65$ (7.80), $\log K_2 = 6.34$ (6.21), $\log K_3 = 4.34$ (4.09). Shown in Fig. 3b are individual UV-VIS spectra of the four Ni(II)–en_n ($n = 0, 1, 2, 3$) complexes.

From Fig. 2b, it is evident that at stoichiometries of [en]/[Ni] ≥ 3, Ni(II) is present almost entirely as $Ni(II)(en)_3$, with only a very small concentration of $Ni(II)(en)_2$ and insignificant amounts of $Ni(II)(en)_1$ present. The UV-VIS spectra of solutions with [en]/[Ni] > 3, normalized to constant concentration, are virtually identical, confirming this conclusion. This fact is also reflected in the abrupt plateau of $[R_{1p}]$ at [en]/[Ni] ≥ 3. Correspondingly, the molar relaxivity of $Ni(II)(en)_3$ can be calculated directly from the measured R_{1p} of the solutions with [en]/[Ni] > 3, giving $[R'''_{1p}]_0 = 149\ M^{-1}\ s^{-1}$ (the subscript zero denotes the zfs-limit).

The measured R_{1p} in the absence of added [en] gave the

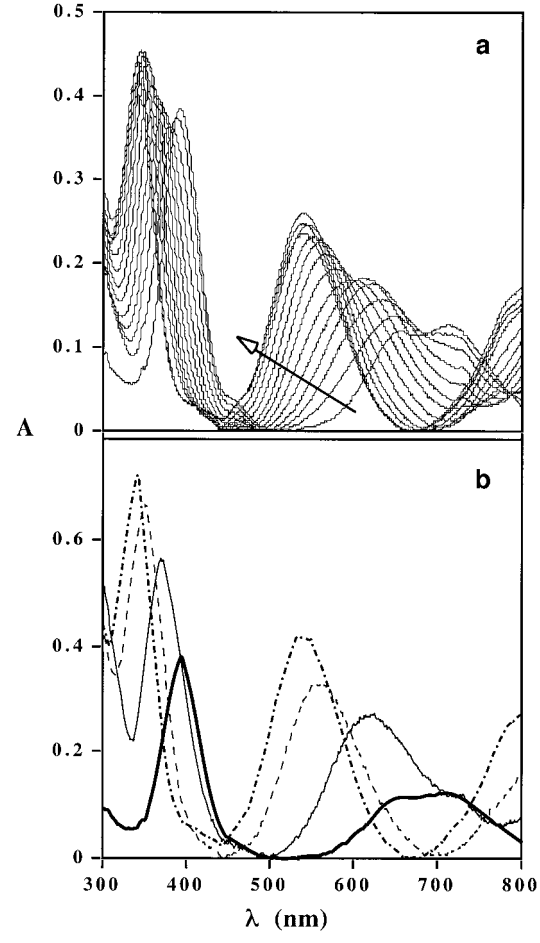

FIG. 3. UV-visible spectra (absorbance vs wavelength) of the titration experiment of Fig. 2a. (a) UV-VIS spectra corresponding to successive points in Fig. 2a, with increasing [en]/[Ni] as indicated by the arrow (the final spectra overlap and are indistinguishable when corrected for dilution). (b) UV-visible spectra normalized to 60 mM Ni(II), of the complexes $[Ni(II)(en)_n(H_2O)_{6-2n}]^{2+}$, for $n = 0$ (bold solid line), $n = 1$ (fine solid line), $n = 2$ (dashes), and $n = 3$ (dash–dot).

TABLE 1

Zfs-Limit Molar T_1 Relaxivities, $[R_{1p}^n]_0$, for the Complexes $[Ni(II)(en)_n(H_2O)_{6-2n}]^{2+}$ (n = 0, 1, 2, 3) in Mixed ^2H_2O/Dioxane (80/20 v/v) Solvent

$Ni(II)(en)_n$	$[R_{1p}^n]_0$	D (cm^{-1})	E (cm^{-1})	$\tau_{S,c}^{(o)}$ (ps)	Δ_T^2 (cm^{-2})	τ_v (ps)
n = 0	74	—	—	—	—	—
n = 1	21	—	—	—	—	—
n = 2 (*35*)	28	7.0	0.482	20	0.68	3.8
n = 3	149	1.7	0.0	27	0.59	2.0

Note. $[R_{1p}^n]_0$ (in units of s^{-1} M^{-1}) was measured from the R_{1p} titration data in Fig. 2. Tabulated values of the static (D, E) and dynamic (Δ_T^2, τ_v) zfs parameters of the *bis*– and *tris*–en complexes were determined from SD/MD simulations of the data in Fig. 4. $\tau_{S,c}^{(o)}$ is the zfs-limit electron spin relaxation time, calculated from Δ_T^2 and τ_v as described in the text.

relaxivity of the uncomplexed Ni(II) cation, $[R_{1p}^0]_0$ = 74 M^{-1} s^{-1}. The relaxivity of the *mono*–en complex was calculated from the measured R_{1p} at a stoichiometry of [en]/[Ni] = 0.25, where only *mono*–en complex and the uncomplexed Ni(II) cation are present in significant concentration. The relaxivity of the *bis*–en complex was calculated at a stoichiometry [en]/[Ni] = 2.0, where the predominant species is $Ni(II)(en)_2$ with 8.6 mol% each of $Ni(II)(en)_1$ and $Ni(II)(en)_3$. The zfs-limit relaxivity of the *bis*–en complex, $[R_{1p}'']_0$ = 28 M^{-1} s^{-1}, was calculated from the measured R_{1p} of this solution after correcting for the relaxation contributions of the *mono*– and *tris*–en species. The zfs-limit molar relaxivities are summarized in Table 1. The solid curve in Fig. 2a was calculated from these molar relaxivities and the molar concentrations of Fig. 2b.

Magnetic Field Dispersion Profiles

Plots of $[R_{1p}]$ as a function of Zeeman field strength at constant temperature are called magnetic field dispersion profiles of the NMR-PRE. Figure 4 shows T_1 fdps (corrected for the diamagnetic background and expressed on a molar basis) produced by the *bis*–(en) (open circles) and *tris*–(en) (solid circles) complexes in the dioxane proton resonance of the mixed ^2H_2O/dioxane solvent. The *tris*–(en) sample was prepared by dissolving recrystallized solid $[Ni(II)(en)_3] \cdot (NO_3)_2$ in the mixed solvent in the presence of one molar excess (en). In this sample, the *tris*–(en) complex was the only significant (>99.9%) Ni(II)-containing species. (This conclusion was tested experimentally by monitoring the effects on $[R_{1p}]$ and on the UV-VIS spectrum of serial additions of excess (en) to the *tris*–en sample. At mole ratios of [en]/[Ni] $\geq$ 3.5, no changes occurred after correction to constant concentration.) The *bis*–(en) sample was prepared by dissolving recrystallized $[Ni(II)(en)_2(H_2O)_2] \cdot Cl_2$ into the mixed solvent to a final Ni(II) concentration of 40 mM. This sample contained the *mono*– and *tris*–(en) complexes in equal concentration as minor species at mole fractions equal to 0.103 times that of the *bis*–(en) complex. The *tris*–(en) contribution to $[R_{1p}]$ has been subtracted from the *bis*–(en) fdp in Fig. 4. No correction was made for *mono*–(en), and the fdp-labeled "*bis*" thus contains a 10% admixture of the *mono*–(en) fdp (*35*).

The experimental fdps of both the *bis*- and the *tris*–(en) complexes exhibited rising dispersive features (Fig. 4). Expressed as a percentage increase of $[R_{1p}]$ above the zfs-limit value ($[R_{1p}]_0$), the amplitude of the dispersive feature is much larger for the *bis*– than for the *tris*–(en) complex. The difference is emphasized in Fig. 5, which compares fdps which are normalized to unity in the zfs-limit. In range B_0 = 0–1.0 T, $[R_{1p}]'$ of the *tris*– complex is almost field-independent, rising by about 5%, while $[R_{1p}]'$ of the *bis*–(en) complex more than doubles. Above 1 T, $[R_{1p}]'$ of both the *bis*– and the *tris*–(en) complexes are significantly field-dependent, but the percentage increase of $[R_{1p}]'$ for the *bis*–(en) complex is several-fold larger than for the *tris*–(en) complex. Not only does the *bis*–(en) fdp exhibit much stronger field dependence than that of *tris*–(en), but also the onset of observable field dependence occurs at a lower field strength (approx. 0.2 T for *bis*–(en) versus 1.0 T for *tris*–(en)).

Figure 6 shows fdps for *tris*–(en) in two other solvent systems. The circles represent the T_1 fdp for water solvent protons in aqueous solution, and the diamonds are an fdp for DMSO protons in DMSO solution. The molar relaxivity, $[R_{1p}''']_0$, calculated from the R_{1p} data of Fig. 6, is approximately the same for the DMSO data as for the dioxane fdp in Fig. 4. For the water proton data (Fig. 6), $[R_{1p}''']_0$ is somewhat larger,

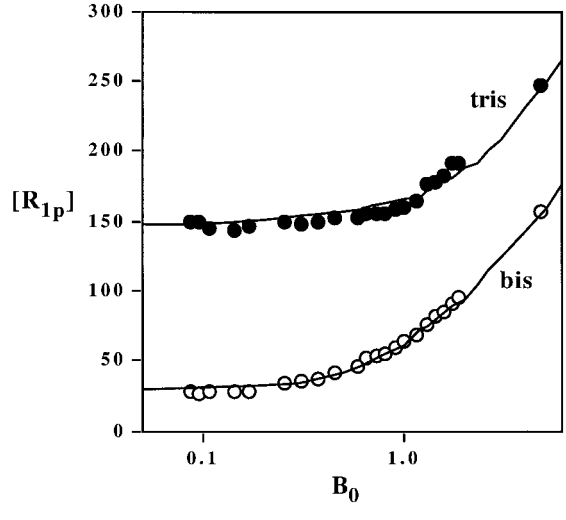

FIG. 4. T_1 field dispersion profiles for Ni(II)–$(en)_2$ (open circles) and Ni(II)–$(en)_3$ (solid circles) dissolved in a mixed dioxane/^2H_2O solvent (20/80 v/v). $[R_{1p}]$ (s^{-1} M^{-1}) is the molar T_1 relaxivity of the dioxane protons after correction for the diamagnetic background and, in the case of the *bis* data, for minor concentration due to *tris* (see text). Solid curves are results of SD/MD simulations computed using parameters given in the table, plus the following: the sum of solvent and solute self-diffusion coefficients, $D_{12} = 1.73 \times 10^{-9}$ m^2 s^{-1}; the reorientational correlation time, $\tau_R^{(2)}$ = 60 ps; the distance of closest approach, d_c = 0.36 nm.

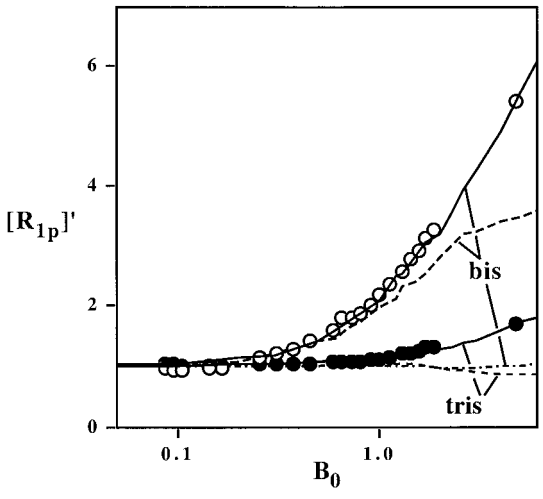

FIG. 5. $[R_{1p}]$ field dispersion profiles of Fig. 4, normalized to unity in the zfs-limit ($[R_{1p}]'$ is unitless). Open and solid circles are experimental data for the *bis*– and *tris*–en complexes. Solid curves are results of best-fit SD/MD simulations. Dashed curves were simulated assuming that electron spin relaxation times are magnetic field independent, $\tau_S = \tau_S^{(0)}$, using the values in Table 1; other parameters were those given in the table and in the legend of Fig. 4. Dash–dot curve for *bis*–en assumes $\tau_S = \tau_S^{(0)}$ and $E = 0$ with other parameters the same as for the *bis*–en solid curve.

197 M^{-1} s^{-1}, than the dioxane value. It is interesting that the DMSO data of Fig. 6, like the dioxane data of Fig. 4, exhibit a dispersion which rises with increasing B_0, while the water proton data exhibit a falling dispersion. For all three *tris*–(en) fdps (Figs. 4 and 6), the fractional change in $[R_{1p}]'$ is several-fold smaller than the corresponding change in the *bis*–(en) fdp (Fig. 5).

Results of SD Simulations

The fdps were analyzed quantitatively using spin dynamics simulation methods described above. Best-fit simulations are shown as solid lines in Fig. 5 (the corresponding theoretical parameters are given in the table and figure legends). Another set of SD simulations (dashed lines) was performed in which the parameters were taken to be the same as for the best-fit simulations, except that the electron spin relaxation time, $\tau_{S,c}$, was held constant, equal to the zfs-limit value, $\tau_{S,c}^{(o)}$ (Table 1). The difference between the solid and dashed simulations in Fig. 5 represents the effect on the fdp of magnetic field-dependence in $\tau_{S,c}$. The dash–dot curve in Fig. 5 is the result of a third simulation for the *bis* complex in which the parameter set was the same as for the best-fit simulation except that zfs rhombicity was set to zero and $\tau_{S,c} = \tau_{S,c}^{(o)}$ was taken to be constant. This third fdp is essentially field-independent, indicating that for the *bis*– complex, the observed field dependence of $[R_{1p}]$ is due almost entirely to the effects of zfs rhombicity and to magnetic field dependence in $\tau_{S,c}$. For the *tris*– complex, the simulated fdp exhibits a mild downward dispersion when $\tau_{S,c}$ is taken to be field-independent (dashed curve in Fig. 5). This feature is a quantization-type dispersion (*25*) which occurs when the Zeeman and zfs energies are of comparable magnitude. No corresponding feature is apparent in the *bis*–(en) fdp calculated with $E = 0$ and constant $\tau_{S,c}$ (dash–dot curve, Fig. 5) because the zfs *D*-value in the *bis*–(en) simulations is fourfold larger than in the *tris*–(en) simulations (7 cm^{-1} vs 1.7 cm^{-1}), displacing the requantization phenomenon to a higher value of the Zeeman field. The difference in *D*-values is expected from the higher symmetry of *tris*–(en) coordination sphere, which contains six chemical equivalent nitrogen atoms, relative to *bis*–(en), which contains 4-N and 2-O donor atoms.

From the simulations in Fig. 5, it is apparent that below 1 T, nearly all of the magnetic field dependence in $[R_{1p}]$ results from the effect of zfs rhombicity and is consequently substantial for *bis*–(en) but nearly absent for *tris*–(en). Above 1 T, significant magnetic field dependence in $[R_{1p}]$ results both from zfs-rhombicity (for *bis*–(en)) and from magnetic field dependence in $\tau_{S,c}$ (for both complexes). The experimental results, taken together with the results of the SD simulation studies, are in agreement with theoretical prediction; namely that for the *bis*–(en) complex, zfs rhombicity causes a substantial depression (3.5- to 4-fold) in $[R_{1p}]$ relative to the zfs-limit. This depression is relieved when the Zeeman energy exceeds the rhombic zfs splitting. The *tris*–(en) fdp exhibits a much milder rising dispersion which is attributable almost entirely to the effects of magnetic field dependence in $\tau_{S,c}$.

DISCUSSION

The two complexes, $[Ni(II)(en)_2(H_2O)_2]^{2+}$ and $[Ni(II)(en)_3]^{2+}$, were selected for study based on the difference in point group symmetry of the zfs tensors. The *bis*–en complex has an orthorhombic zfs tensor (D_{2h}), while the *tris*–en com-

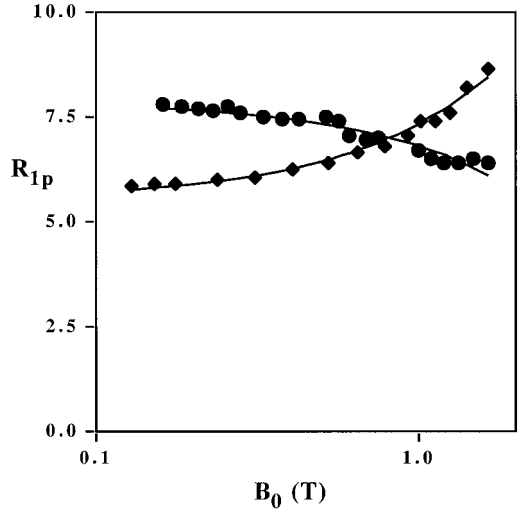

FIG. 6. R_{1p} (s^{-1}) field dispersion profiles of $[Ni(II)(en)_3]^{2+}$, measured at 20°C in aqueous solution (circles) and in DMSO (diamonds). Solutions contain 40 mM *tris*–(en) complex plus an equimolar quantity of excess (en).

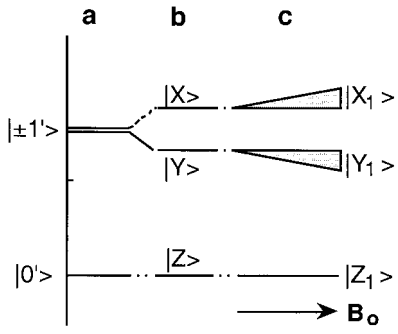

FIG. 7. Spin energy level diagram for $S = 1$. (a) The cylindrical zfs-limit. (b) The orthorhombic zfs-limit. (c) The orthorhombic zfs-limit of a powder in the presence of a Zeeman field.

plex has a cylindrical zfs tensor, $D_{\infty h}$ (the point groups describe the zfs tensor). When present, zfs rhombicity has been predicted to have a controlling influence on the magnitude of the zfs-limit NMR-PRE and on the shape of the T_1 field dispersion profile. For $S = 1$, the orthorhombic zfs term depresses the zfs-limit NMR-PRE strongly (several-fold) relative to the cylindrical zfs tensor case. This depression is confirmed in the $[R_{1p}]_0$ data of Table 1, where $[R'_{1p}]_0$ and $[R''_{1p}]_0$ are both much smaller, by factors of 7 and 5, respectively, than $[R'''_{1p}]_0$. Measurements of $[R'''_{1p}]_0$ in a pure aqueous solvent and in DMSO (Fig. 6) likewise gave values comparable to or greater than $[R'''_{1p}]_0$ in the mixed solvent.

When, with increasing Zeeman field strength, the Zeeman energy becomes comparable to the smallest zfs-splittings, the spin wave functions change profoundly, and as a consequence the NMR-PRE rises dramatically. The predicted rise in $[R_{1p}]_0$ for orthorhombic Ni(II) complexes has been observed in prior studies (*10, 12, 13, 15, 28, 29*), but the contrary case, where an $S = 1$ complex with a cylindrical zfs tensor does not exhibit this feature in the fdp, has not previously been reported. Figures 4 and 5 present such a comparison, with results that are consistent with theoretical expectation. (It should be emphasized that the characteristic properties of the NMR-PRE depend strongly on spin value and that the behavior of $S = 1$ is rather different from that of other spin values.).

Relaxation Mechanism for S = 1

The NMR relaxation mechanism produced by an electron spin $S = 1$ has been described elsewhere (*10*). We give here a brief account of the mechanism that focuses on the role of zfs tensor symmetry. The zfs-limit spin energy levels are shown for a cylindrical zfs tensor in Fig. 7a and for an orthorhombic zfs tensor in Fig. 7b. In the cylindrical case, the $m_S = \pm 1$ levels are degenerate and are separated from the $m_S = 0$ level by a splitting equal to the cylindrical zfs parameter, D. The spin motion in the cylindrical zfs-limit is "precession-like" in that the motion is quantized spatially along the principal axis of the zfs tensor (the molecule-fixed $\hat{z}$-axis), with $\langle S_{\hat{z}} \rangle$ a constant of the motion (the Larmor precession and the cylindrical zfs-limit precession are compared in Figs. 8a and 8b). The T_1 NMR-PRE is produced by frequency components of the dipolar field of $\langle \mathbf{S} \rangle$ that are resonant with the nuclear spin motions, which are very slow (essentially zero frequency) compared to the motions of the electron spin TCFs. The dipolar field of $\langle \mathbf{S} \rangle$ is a sum of the dipolar fields associated with the Cartesian spin components, the motion of which is described by the TCFs, $G_{\hat{r}}(t) = \overline{\langle S_{\hat{r}}(t) \cdot S_{\hat{r}}(0) \rangle}$ ($\hat{r} = \hat{x}, \hat{y}, \hat{z}$). In the cylindrical zfs-limit, $G_{\hat{z}}(t)$ and $\langle S_{\hat{z}} \rangle$ are constants of the motion while $G_{\hat{x}}(t)$ and $G_{\hat{y}}(t)$ oscillate at the 1Q transition frequency ω_D.

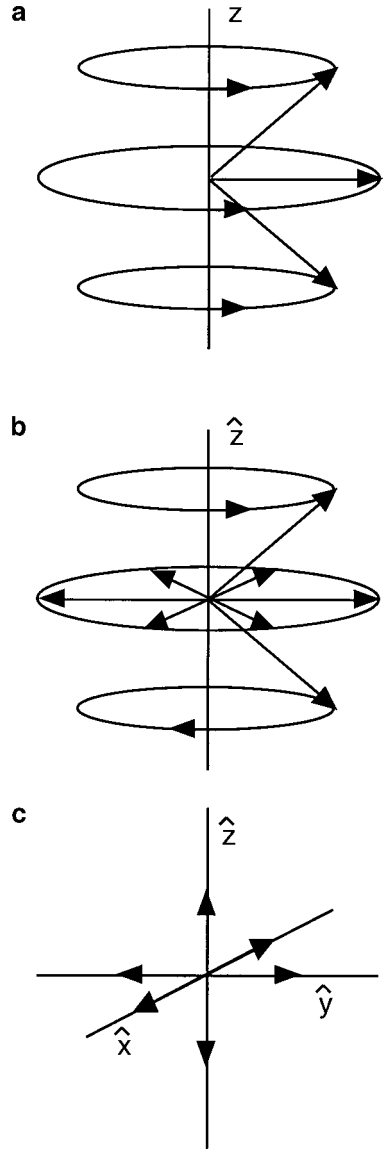

FIG. 8. Semi-classical precessional (oscillational) picture for $S = 1$ driven by a (a) Zeeman interaction; (b) cylindrical zfs interaction; (c) orthorhombic zfs interaction. The z-axis in (a) is the axis of the laboratory magnetic field, while the $\hat{x}$, $\hat{y}$, $\hat{z}$-axes in (b) and (c) are principal axes of the molecule-fixed zfs-tensor.

Thus the dipolar field associated with $G_{\hat{z}}(t)$ is precessionally static and has a much larger component at $\omega = 0$ than do the dipolar fields associated with $G_{\hat{x}}(t)$ and $G_{\hat{y}}(t)$, which are thus, in effect, "motionally-decoupled" from I. In the cylindrical zfs-limit, most of the NMR relaxation efficiency results from pathways involving $G_{\hat{z}}(t)$.

Zfs-rhombicity changes this picture dramatically by driving $G_{\hat{z}}(t)$ into oscillation. These oscillations result from changes in the spin eigenfunctions, labeled as in Fig. 7b. In the cylindrical zfs-limit, the spin eigenfunctions can be (and usually are) chosen as the circularly polarized set $\{|+1'\rangle, |0'\rangle, |-1'\rangle\}$, where the prime indicates that the functions are spatially quantized in the molecular frame rather than the laboratory frame. However, since $|+1'\rangle$ and $|-1'\rangle$ are degenerate, the eigenfunctions could alternatively be chosen in the molecule-fixed Cartesian representation,

$$|X\rangle = -2^{-1/2}(-|+1'\rangle + |-1'\rangle)$$
$$|Y\rangle = +2^{-1/2}(-|+1'\rangle - |-1'\rangle)$$
$$|Z\rangle = |0'\rangle.$$

In the circular basis under a cylindrical zfs driving force, $\langle S_{\hat{z}}\rangle$ is diagonal, with matrix elements equal to $m_S = +1, 0, -1$ in the three eigenstates.

The presence of an orthorhombic zfs component (which results from chemical inequivalence of $\hat{x}$ and $\hat{y}$) breaks the degeneracy of $|\pm 1'\rangle$ and forces a Cartesian polarization on the spin eigenfunctions (Fig. 7b). In the Cartesian eigenbasis, the component spin matrices, $\{\langle S_{\hat{x}}\rangle, \langle S_{\hat{y}}\rangle, \langle S_{\hat{z}}\rangle\}$ are all off-diagonal. The only nonvanishing matrix elements of $\langle S_{\hat{x}}\rangle$ are those coupling $|Y\rangle$ and $|Z\rangle$; and more generally, $\langle \hat{q}|S_{\hat{r}}|\hat{s}\rangle$ is nonvanishing only if $\{\hat{q}, \hat{r}, \hat{s}\}$ are all different. The component TCFs oscillate at the corresponding transition frequencies. Thus $G_{\hat{z}}(t)$ oscillates at the $\{|X\rangle \leftrightarrow |Y\rangle\}$ transition frequency, etc. Whereas in the cylindrical zfs-limit, $|X\rangle$ and $|Y\rangle$ are degenerate and hence $\langle S_{\hat{z}}\rangle$ is constant in time, in the orthorhombic zfs-limit the degeneracy is broken, and the nonvanishing matrix elements of $\langle S_{\hat{z}}\rangle$ oscillate at the $\{|X\rangle \leftrightarrow |Y\rangle\}$ transition frequency, $2\omega_E$. The semi-classical picture of the spin motion changes from "precession-like" in the cylindrical zfs-limit (Fig. 8b), to the picture of Fig. 8c in the orthorhombic zfs-limit, where the Cartesian spin components undergo linear oscillations at incommensurate frequencies which are determined by the level splittings (Fig. 7b). The rhombicity-induced oscillation in $G_{\hat{z}}(t)$ decouples I from S (a kind of motional decoupling), thereby suppressing the NMR-PRE, often profoundly, relative to the cylindrical zfs-limit. This suppression is reflected in the small observed values of $[R'_{1p}]_0$ and $[R''_{1p}]_0$ relative to $[R'''_{1p}]_0$ (Table 1).

The addition of a small Zeeman interaction (Fig. 7c), comparable in magnitude to the *intra*doublet ($|X\rangle \leftrightarrow |Y\rangle$) splitting ($2\omega_E$) but smaller than the *inter*doublet ($|Y\rangle$, $|X\rangle \leftrightarrow |Z\rangle$) splittings ($\omega_D \pm \omega_E$), introduces net circular character into the spin eigenfunctions. As a consequence, diagonal matrix elements grow into $\langle S_{\hat{z}}\rangle$, and the NMR relaxation efficiency increases approximately as the squares of the matrix elements. This phenomenon is responsible for the major portion of the large, rising dispersion that is present in the fdp of Ni(II)–$(en)_2$. A similar feature is present in all prior published Ni(II) fdp data involving orthorhombic zfs tensors (*10, 12, 13, 15, 28, 29*). That this phenomenon is absent only for $[Ni(II)(en)_3]^{2+}$ provides strong support for the conclusion that it originates in the orthorhombic zfs interaction.

EXPERIMENTAL

The complexes $[Ni(II)(en)_n(H_2O)_{6-2n}]^{2+}$ ($n = 0, 1, 2, 3$) form a stepwise series, the formation constants of which have been reported (*30*) in water and in mixed water/dioxane solution. In the R_{1p} titration experiment, 25-μL aliquots of a stock solution of 15 mM ethylenediamine dissolved in the mixed dioxane/^2H_2O solvent (25/75 v/v) were added to a 500-μL NMR sample containing 60 mM Ni(II)Cl_2 in the same solvent. During this procedure, the initial dark green solution of Ni^{2+} changes color through shades of blue and then violet. The dioxane proton R_{1p} was measured at 10.6 MHz, 20°C, after each addition. UV-VIS spectra were also recorded in a parallel titration experiment.

For NMR field dispersion profile studies, solutions at [en/Ni] mole ratios, $\rho = 2$ and $\rho = 4$, were prepared separately in the mixed ^2H_2O/dioxane solvent. The *tris*–en complex was prepared (*27*) by dropwise addition of ethylenediamine to an aqueous solution of 3.0 M $Ni(NO_3)_2$, added to a final stoichiometry of [en/Ni] = 4.0. This complex was crystallized under vacuum, dried, and then redissolved in the mixed solvent to which excess (en) was added in equal molar ratio to Ni(II). The final concentration of [Ni(II)] was 29 mM. The *bis*–en complex was prepared by addition of (en) to $NiCl_2$ to a final stoichiometry of –/[Ni(II)] = 2.0 and then crystallized under vacuum. This solid was redissolved in the mixed solvent to a final concentration of 23 mM [Ni(II)]. The diamagnetic R_1 background was measured at each magnetic field strength using a sample of the mixed solvent (20°C). The background R_1 was slightly field-dependent, varying from 0.334 s^{-1} at 0.082 T to 0.28 s^{-1} MHz at 4.5 T.

Control experiments were run to test whether the Cl^- counterion enters the Ni(II) coordination sphere on the *bis*–en complex. In these experiments, changes in R_{1p} and in the UV-VIS spectra were monitored upon addition of excess Cl^- added as NaCl (aq). Neither R_{1p} nor the UV-VIS spectrum, adjusted to constant concentration, was significantly affected by added Cl^-. Furthermore, the UV-VIS spectra and R_{1p} were the same in comparable samples containing either NO_3^- or Cl^- as counterion.

The T_1 magnetic field dispersion profile (fdp) of the solvent peak was measured in the range 0.0822–1.83 T using a home-

built tunable NMR relaxation spectrometer (*24*). T_1 was measured using the phase-shifted triplet sequence (*37*), $(\pi)_0$–$[\tau_d$–$(\pi/2)_0$–τ_{tr}–$(\pi)_\pi$–τ_{tr}–$(\pi/2)_0]_n$, in which the magnetization is initially inverted by the $(\pi)_0$ pulse and, at intervals of τ_d, periodically sampled by the pulse triplet, $[(\pi/2)_0$–τ_{tr}–$(\pi)_\pi$–τ_{tr}–$(\pi/2)_0]$, which tilts the magnetization from the z-axis to the $x-y$ plane, refocuses it with the π_π pulse, and returns it to the z-axis with the $(\pi/2)_0$ pulse applied at the spin echo. In order that the sampling triplet causes little perturbation of the decaying magnetization, τ_{tr} is set to be short compared to τ_d, typically, $\tau_{tr} < 0.01\ \tau_d$. The temperature was maintained at 20.0 ± 0.2°C by a stream of dry nitrogen and checked periodically with a calibrated thermistor in a dummy sample. The repeatability of the T_1 measurement on a given sample was ±1%. T_1 measurements at 4.7 T were carried out by inversion-recovery using a commercial high-resolution spectrometer, but the measurement accuracy was significantly poorer (±7%), primarily due to less accurate temperature control (±3°C).

APPENDIX

Electron Spin Relaxation outside the Zeeman Limit

The quantities, $\tau_{S,r}$, used in the spin dynamics simulations are decay constants for the rotating-frame time correlation functions,

$$G_r(t) = \overline{\langle S_r^*(t) \cdot S_r^*(0)\rangle} \quad (r = x, y, z), \qquad [A1]$$

of the electron spin components, defined as

$$(\tau_{S,r})^{-1} = -\langle S_r^2\rangle^{-1} \frac{d}{dt} \overline{\langle S_r^*(t) \cdot S_r^*(0)\rangle}. \qquad [A2]$$

Assuming that the electron spin density matrix ρ_S remains at its thermal equilibrium value, ρ_S°, Eq. [A2] can be written, after invoking closure, as

$$(\tau_{S,r})^{-1} = -\langle S_r^2\rangle^{-1} \sum_{\alpha,\beta} (\rho_S^\circ)_{\alpha\alpha} \overline{\left(\frac{d(S_r^*(t))_{\alpha\beta}}{dt}\right)_0 (S_r)_{\beta\alpha}}, \qquad [A3]$$

where the electron spin eigenstates are labeled a, b and the superscripting line denotes a spatial average. We assume that the total electron spin Hamiltonian, H_S, has a static part composed of a sum of the Zeeman Hamiltonian and the collisionally averaged zfs Hamiltonian, $H_S^\circ = H_{Zeem} + H_{zfs}^\circ$. The spin relaxation mechanism that is described by $\tau_{S,r}$ results from collisional modulation of the zfs tensor, a process described by the stochastic Hamiltonian, $H'_{zfs}(t)$. (In addition to collisional zfs modulation, reorientational modulation of H_{zfs}° provides an additional electron spin relaxation pathway, the effects of which are evaluated explicitly in the time domain by the algorithms of SpinDyn.f (see above)). Neglecting zfs tensor components of higher order than second (which is rigorously valid for $S < 2$), $H'_S(t)$ can be written as a sum of molecular-frame cartesian terms,

$$\begin{aligned}\hbar^{-1} H'_S(t) &= \sum_q c_q(t) S_q^{(2)} \\ &= c_{\hat{z}^2}(t) S_{\hat{z}^2} + c_2(t) S_{\hat{x}^2-\hat{y}^2} \\ &\quad + c_{\hat{x}\hat{y}}(t) S_{\hat{x}\hat{y}} + c_{\hat{x}\hat{z}}(t) S_{\hat{x}\hat{z}} + c_{\hat{y}\hat{z}}(t) S_{\hat{y}\hat{z}}. \end{aligned} \qquad [A4]$$

The quadratic spin operators, $S_q^{(2)}$, are cartesian tensor operators defined as

$$\begin{aligned} S_{\hat{z}^2} &= (3/2)^{1/2}(S_{\hat{z}}^2 - S(S+1)/3) \\ S_{\hat{x}^2-\hat{y}^2} &= 2^{-1/2}(S_{\hat{x}}^2 - S_{\hat{y}}^2) \\ S_{\hat{x}\hat{z}} &= 2^{-1/2}(S_{\hat{x}} S_{\hat{z}} + S_{\hat{z}} S_{\hat{x}}), \text{ etc.} \end{aligned} \qquad [A5]$$

We use labels $q = \{1, 2, 3, 4, 5\}$ for $\{z^2, x^2 - y^2, xy, xz, yz\}$. The coefficients, $c_q(t)$, have stochastic time dependence given by

$$\overline{c_q(t) c_{q'}(0)} = \overline{|c_q|^2} \exp(-t/\tau_q) \delta_{q,q'}, \qquad [A6]$$

where in general the amplitudes and decay constants of the different modes are distinct. The simulations of Fig. 6 assumed that all $\overline{|c_q|^2}$ and all τ_q are equal.

Expressions for the matrix elements in Eq. [A3] have been derived from the operator equation

$$\frac{dS_r^*(t)}{dt} = i\hbar^{-1}[H'_S(t), S_r^*(t)], \qquad [A7]$$

using second-order time-dependent perturbation theory, following a procedure analogous to that of Redfield theory. In particular, the Redfield assumption that the zfs correlation times are shorter than the electron spin relaxation times, $\tau_q \ll \tau_{S,r}$, is invoked. The resulting expression for the relaxation rates is

$$\begin{aligned}(\tau_{S,\hat{r}})^{-1} &= 3(S(S+1))^{-1}(2S+1)^{-1}[\sum_q \overline{|c_q|^2} n_q^{(r)} \\ &\quad \times \sum_{\alpha,\beta} |\langle\alpha|S_q|\beta\rangle|^2 j_q(\omega_{\alpha\beta}) + C], \end{aligned} \qquad [A8]$$

with

$$\begin{aligned} C &= 3^{1/2} \sum_{\alpha,\beta} [\overline{|c_1|^2} \langle\alpha|S_1|\beta\rangle\langle\beta|S_2|\alpha\rangle j_1(\omega_{\alpha\beta}) \\ &\quad + \overline{|c_2|^2} \langle\alpha|S_2|\beta\rangle\langle\beta|S_1|\alpha\rangle j_2(\omega_{\alpha\beta})], \\ j_q(\omega) &= \tau_q/(1 + \omega^2\tau_q^2). \end{aligned} \qquad [A9]$$

Equation [A8] assumes the high temperature limit of the density matrix, where $(\rho^{\circ})_{\alpha\alpha} = (2S + 1)^{-1}$. The coefficients $n_q^{(r)}$ are defined in terms of the spin double commutators,

$$[S_r, [S_r, S_q]] = n_q^{(r)} S_q + n_{q'}^{(r)} S_{q'}, \qquad [A10]$$

the evaluation of which is straightforward. For $r = z$, coefficients $n_q^{(r)}$ for $q = \{1 \ldots 5\}$ equal $\{0, 4, 4, 1, 1\}$, respectively. For $r = x$ and y, $n_q^{(x)} = \{3, 1, 1, 1, 4\}$ and $n_q^{(y)} = \{3, 1, 1, 4, 1\}$. The second term on the r.h.s. of Eq. [A10] vanishes for $S < 2$.

In SD simulations, Eq. [A8] was used to calculate the three molecular-frame relaxation times, $\tau_{S,\hat{r}}$. These quantities were subsequently converted to laboratory-frame relaxation times, τ_{Sx} and τ_{Sz}, by using an appropriate averaging procedure involving three separate calculations in which first $\hat{x}$, then $\hat{y}$, then $\hat{z}$ (the circumflexes ($\wedge$) indicating molecule-fixed axes) were aligned along the Zeeman field direction (z). The lab-frame quantity, τ_{Sz}^{-1}, was then computed as one-third the sum of $\tau_{S,\hat{x}}^{-1}$ from the first calculation, $\tau_{S,\hat{y}}^{-1}$ from the second calculation, and $\tau_{S,\hat{z}}^{-1}$ from the third. A parallel procedure was used to calculate τ_{Sx}^{-1}.

ACKNOWLEDGMENT

This research was supported by the U.S. National Science Foundation in the form of a research grant, CHE-9423351.

REFERENCES

1. I. Solomon, *Phys. Rev.* **99,** 555 (1955).
2. N. Bloembergen, *J. Chem. Phys.* **27,** 572, 595 (1957).
3. N. Bloembergen and L. O. Morgan, *J. Chem. Phys.* **34,** 842 (1961).
4. R. R. Sharp, *J. Chem. Phys.* **93,** 6921 (1990).
5. T. Bayburt and R. R. Sharp, *J. Chem. Phys.* **92,** 5892 (1990).
6. R. R. Sharp, *J. Magn. Reson.* **100,** 491 (1992).
7. R. R. Sharp, *J. Chem. Phys.* **98,** 2507 (1993).
8. R. R. Sharp, *J. Chem. Phys.* **98,** 6092 (1993).
9. J.-M. Bovet and R. R. Sharp, *J. Chem. Phys.* **99,** 18 (1993).
10. R. R. Sharp, S. M. Abernathy, and L. L. Lohr, *J. Chem. Phys.* **107,** 7620 (1997).
11. S. M. Abernathy and R. R. Sharp, *J. Chem. Phys.* **106,** 9032 (1997).
12. S. M. Abernathy and R. R. Sharp, *J. Phys. Chem. A* **101,** 3692 (1997).
13. S. M. Abernathy, J. C. Miller, L. L. Lohr, and R. R. Sharp, *J. Chem. Phys.* **109,** 4035 (1998).
14. P.-O. Westlund has reviewed Swedish work prior to 1995 on the Stochastic Liouville/Pseudorotation Model *in* "Dynamics of Solutions and Fluid Mixtures by NMR" (J. J. Delpuech, Ed.), p. 173, Wiley, New York, 1995.
15. T. Larsson, P.-O. Westlund, J. Kowalewski, and S. H. Koenig, *J. Chem. Phys.* **101,** 1116 (1994).
16. J. Svoboda, T. Nilsson, J. Kowalewski, P.-O. Westlund, and P. T. Larsson, *J. Magn. Reson. A* **121,** 108 (1996).
17. P.-O. Westlund, *Mol. Phys.* **85,** 1165 (1995).
18. M. Odelius, C. Ribbing, and J. Kowalewski, *J. Chem. Phys.* **103,** 1800 (1995); **104,** 96 (1996).
19. E. Strandberg and P.-O. Westlund, *J. Magn. Reson. A* **137,** 333 (1999).
20. P.-O. Westlund, *J. Chem. Phys.* **108,** 4945 (1998).
21. L. Banci, I. Bertini, and C. Luchinat, "Nuclear and Electron Relaxation," VCH, New York, 1991.
22. I. Bertini, O. Galas, C. Luchinat, and G. Parigi, *J. Magn. Reson. A* **113,** 151 (1995).
23. I. Bertini, J. Kowalewski, C. Luchinat, T. Nilsson, and G. Parigi, *J. Chem. Phys.* **111,** 5795 (1999).
24. J. C. Miller, S. M. Abernathy, and R. R. Sharp, *J. Phys. Chem. A* **104,** 4839 (2000).
25. J. C. Miller and R. R. Sharp, *J. Phys. Chem. A* **104,** 4889 (2000).
26. H. Fukui, K. Miura, and H. Matsuda, *J. Magn. Reson.* **88,** 311 (1990).
27. L. Swink and M. Atoji, *Acta Crystallogr.* **13,** 63 (1960).
28. L. Banci, I. Bertini, and C. Luchinat, *Inorg. Chem. Acta* **100,** 173 (1985).
29. L. Banci, I. Bertini, and C. Luchinat, "Nuclear and Electron Relaxation," pp. 134–135, VCH, New York, 1991.
30. L. G. Sillen and A. E. Martell, "Stability Constants of Metal–Ion Complexes," Part B: Organic Ligands (E. Hogfeldt, Ed.), The Chemical Society (London) Spec. Publ., No. 25, 1971.
31. H. C. Torrey, *Phys. Rev.* **92,** 962 (1953).
32. A. Abragam, "The Principles of Nuclear Magnetism," Ch. 8, Oxford Univ., London, 1961.
33. M. Rubinstein, A. Baram, and Z. Luz, *Mol. Phys.* **20,** 67 (1971).
34. A. Carrington and G. R. Luckhurst, *Mol. Phys.* **8,** 125 (1964).
35. Whether the $[Ni(II)(en)_2(H_2O)_2]^{2+}$ complex is present solely as the *trans* isomer or as an equilibrium *cis/trans* mixture is not known with certainty. The analogous $[Ni(II)(en)_2Cl_2]$ and $[Ni(II)(en)_2Br_2]$ complexes both crystallize as *trans* isomers (*36*). If both isomers are present, then the parameters of Table 1 represent an average of two species, both of which possess orthorhombic zfs tensors.
36. A. S. Antsyshkina and M. A. Porai-Koshits, Dokl. Akad. Nauk SSSR (English translation), **143**(1), 105 (1962).
37. A. E. Haddy, W. D. Frasch, and R. R. Sharp, *Biochemistry* **24,** 7926 (1985).